Low Torque Ripple Spoke-type Permanent Magnet Motor for Electric Vehicle

Hoyun Won
Department of Electrical and Computer Engineering and The Center for Advanced Vehicle Technologies (CAVT)
The University of Alabama
Tuscaloosa, AL, USA
hwon@crimson.ua.edu

Yang-Ki Hong
Department of Electrical and Computer Engineering and CAVT
The University of Alabama
Tuscaloosa, AL, USA
ykhong@eng.ua.edu

Woncheol Lee
Department of Electrical and Computer Engineering and CAVT
The University of Alabama
Tuscaloosa, AL, USA
wlee43@crimson.ua.edu

Minyeong Choi
Department of Electrical and Computer Engineering and CAVT
The University of Alabama
Tuscaloosa, AL, USA
mchoi11@crimson.ua.edu

Shuhui Li
Department of Electrical and Computer Engineering and CAVT
The University of Alabama
Tuscaloosa, AL, USA
sli@eng.ua.edu

Hwan-Sik Yoon
Department of Mechanical Engineering and CAVT
The University of Alabama
Tuscaloosa, AL, USA
hyoon@eng.ua.edu

***Abstract*—We have designed a rotor for a spoke-type interior permanent magnet synchronous machine (IPMSM) with rare-earth-free permanent magnets (RE-free PM) to lower torque ripple while maintaining reasonable torque. Three kinds of RE-free PMs, $SrFe_{12}O_{19}$ (SrM ferrite), $Nd_2Fe_{14}B$ (NdFeB), and low-temperature phase (LTP)-MnBi, were used for the designed rotor to evaluate motor performance at 20 °C and 125 °C. The proposed motor with LTP-MnBi for the rotor-core magnet and SrM for the flux-directing magnet shows the increased torque by 7.1 % and 12.5 % at 20 °C and 125 °C, respectively, and decreased torque ripple by 50 % and 62.9 % at 20 °C and 125 °C, respectively, as compared to the conventional rotor. According to the demagnetization analysis, the proposed motor is far less vulnerable to irreversible demagnetization than the conventional motor. This work opens a new avenue in the design of rare-earth-free permanent magnet synchronous motor for electric vehicle applications.**

Keywords—Electric vehicle, interior permanent magnet machine, spoke-type, permanent magnet, and torque ripple

I. Introduction

An interior permanent magnet synchronous machine (IPMSM) with rare-earth (RE) permanent magnet (PM) has been widely adopted in many automotive industries due to its high power density, high efficiency, and wide constant-power operating region. However, price and supply fluctuations of RE minerals, such as dysprosium (Dy) and neodymium (Nd), become issues in maintaining the production of hybrid electric vehicles (HEVs) and electric vehicles (EVs) at constant low cost with reliable supply. Furthermore, the Curie temperature of the Nd-Fe-B PM is relatively lower than those of RE-free permanent magnets. Therefore, RE-free magnet-based IPMSM has received a great deal of attention from academia and industry [1-5].

This work was supported in part by National Science Foundation IUCRC under Grant number IPP-1650564 and Creative Materials Discovery Program through National Research Foundation of Korea (NRF) funded by Ministry of Science, ICT, and Future Planning under Award number 2016M3D1A1027835.

One disadvantage of RE-free PM is its low maximum energy product $(BH)_{max}$ compared to RE magnets. This low $(BH)_{max}$ yields a small resultant air-gap flux, resulting in a lower torque than RE magnets. To compensate for this low air-gap flux, a topology of two adjacent radially arranged PMs with oppositely magnetization directions is used in IPMSM; this is also known as a spoke-type IPMSM (S-IPMSM). Although the S-IPMSM exhibits high torque density, it suffers from high torque ripple [2,3,7].

In a vehicle, the low torque ripple is desired because it not only offers smooth and quiet driving to passengers by reducing noise and vibration, but also reduces the size of the suspension system. The size of the suspension system is proportional to the vibration amplitude [8]. To reduce the torque ripple via motor design approach, numerous methods have been proposed, such as skewing [3], the fractional number of slot per pole [3], and notching [9]. Although these approaches reduce the torque ripple, they reduce the average torque and also demand expensive high precision dies and tools.

The proposed S-IPMSM in this paper has successfully lowered the torque ripple while maintaining competitive torque performance by employing flux-directing (FD) magnets and isosceles trapezoidal-shaped nonmagnetic material without requiring expensive dies and tools. The designed motor was evaluated at 20 °C and 125 °C for its performance with respect to three different PMs: low-temperature phase (LTP)-MnBi and two commercially available PMs such as $SrFe_{12}O_{19}$ (SrM: NMF-12G) and $Nd_2Fe_{14}B$ (NdFeB: Vacodym 890). Then, the demagnetization analysis was performed.

II. Designed Motor Structure and Specification

Fig. 1 shows the rotor configuration of the conventional [1] and proposed motors. Both rotors consist of 8 rotor-core (RC) magnets, each with a cross-sectional area of 908 mm^2. On the

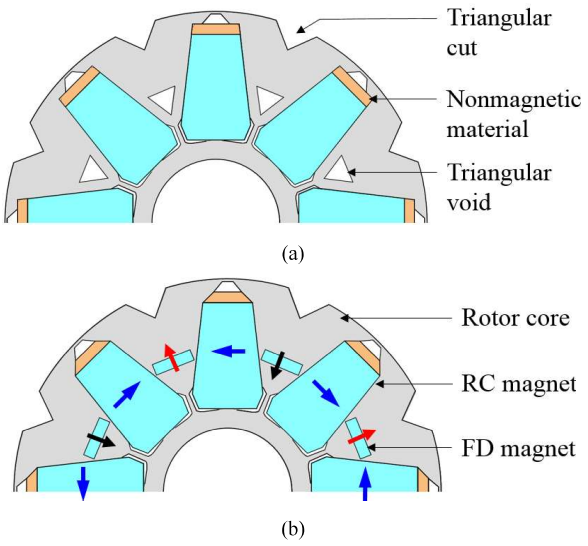

Fig. 1. Rotor structure of (a) conventional and (b) proposed motor.

TABLE I. SPECIFICATION OF THE CONVENTIONAL AND PROPOSED MOTORS

Parameter	Value
Stator outer/inner diameter [mm]	264/161.9
Rotor outer/inner diameter [mm]	160.4/48.5
Stack length [mm]	50.8
Number of poles/slots	8/48
Stator turns per coil	11
Peak current [A_{rms}]	177
Core material	M19-29G

top of each pole in the conventional motor, an 18.6 mm wide and 4 mm long rectangular nonmagnetic material is attached, whereas an isosceles trapezoidal shape with widths of 10.4 mm (top base) and 18.6 mm (bottom base) and a length of 4 mm is used for the proposed motor. The role of the nonmagnetic material is to prevent the tip of the magnet from demagnetizing irreversibly because of the winding flux. On the top of the nonmagnetic material, the isosceles trapezoidal cavity (4.1 mm (top base), 10.4 mm (bottom base), and 3.7 mm (height)) is inserted to ensure a smooth flow of large weakening flux during flux-weakening operation. Between the RC magnets, both designs have the upper triangular air cuts on the edge of the rotor. These cuts help not only to redirect but also to block the unnecessary winding flux that causes torque reduction. Lastly, as illustrated in Fig. 1, in the conventional design, triangular air voids are inserted, whereas the proposed design employs a rectangular magnet (FD magnet: 15 mm (W) × 4 mm (L)) located between each pair of RC magnets. The flux orientation of the RC and FD magnets is shown in Fig. 1 (b). Table I shows that the physical dimensions and operating conditions of the two designs.

To compare the torque and torque ripple of S-IPMSM with triangular cut and void (S-IPMSM-TCV) and S-IPMSM with nonmagnetic cut and FD magnets (S-IPMSM-NCFDM), we

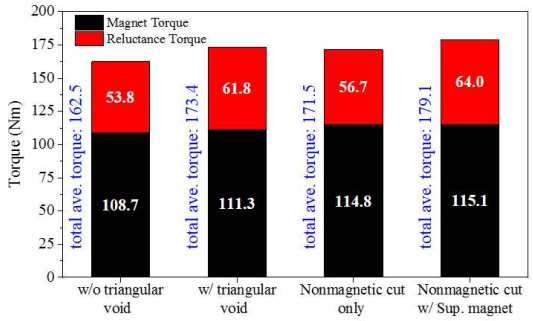

Fig. 2. Torque characteristics of four rotor topologies

TABLE II. MAGNETIC PROPERTIES OF THREE MAGNET TYPES

Parameter	LTP-MnBi	SrM	NdFeB
B_r [Tesla]	0.6	0.44	1.19
H_c [kA/m]	405	340	915
Relative price [/kg]	12.12	1.5	30
T_c [°C]	720	689	493
Reference	[10]	[11]	[12]

have used ANSYS Maxwell v.18.2 based on 2D finite element analysis (FEA). Also, S-IPMSM and S-IPMSM with nonmagnetic cut (S-IPMSM-NC), shown in Fig. 3 (a) and (c), were simulated to observe the effect of the triangular cut, nonmagnetic cut, and FD magnet. In the simulation, three different types of PM such as LTP-MnBi, SrM, and NdFeB were used. The detailed magnetic properties and auxiliary information of the PMs are summarized in Table II. The parameters for each PM are either experimentally verified or obtained from datasheets for commercial products [10-12].

III. RESULTS AND DISCUSSION

In this section, the torque characteristics of the rotor models mentioned above are discussed. Then, the temperature-dependent torque characteristics of the proposed motor are compared with the characteristics of the conventional motor. Lastly, the performance of the proposed spoke-type motor was compared with that of the reported motors.

A. Torque Characteristic and Analysis

The magnetic properties of SrM (RC magnet) and NdFeB (FD magnet) were used for the torque characteristics simulation. All analyses were performed under the assumption that the motor is rotating counter-clockwise (CCW) under motoring operation at 3000 revolutions per minutes (rpm) and maximum current (177 A_{rms}). Fig. 2 shows the torque distributions between magnet (T_m) and reluctance torque (T_r) of four rotor topologies. The insertion of triangular cuts and voids (IPMSM-TCV) increase both the T_m and T_r by 2.3% and 14.0%, respectively, while lowering the torque ripple by 65%. These improvements can be explained by examining the magnetic flux density distribution shown in Fig. 3 (a) and (b). In the black circled area in Fig. 3 (a), the flux from the winding follows through its nearest adjacent slots immediately when the triangular cut is not present. Since the rotor rotates CCW, these flux lines, which rotate clockwise, oppose the rotation by

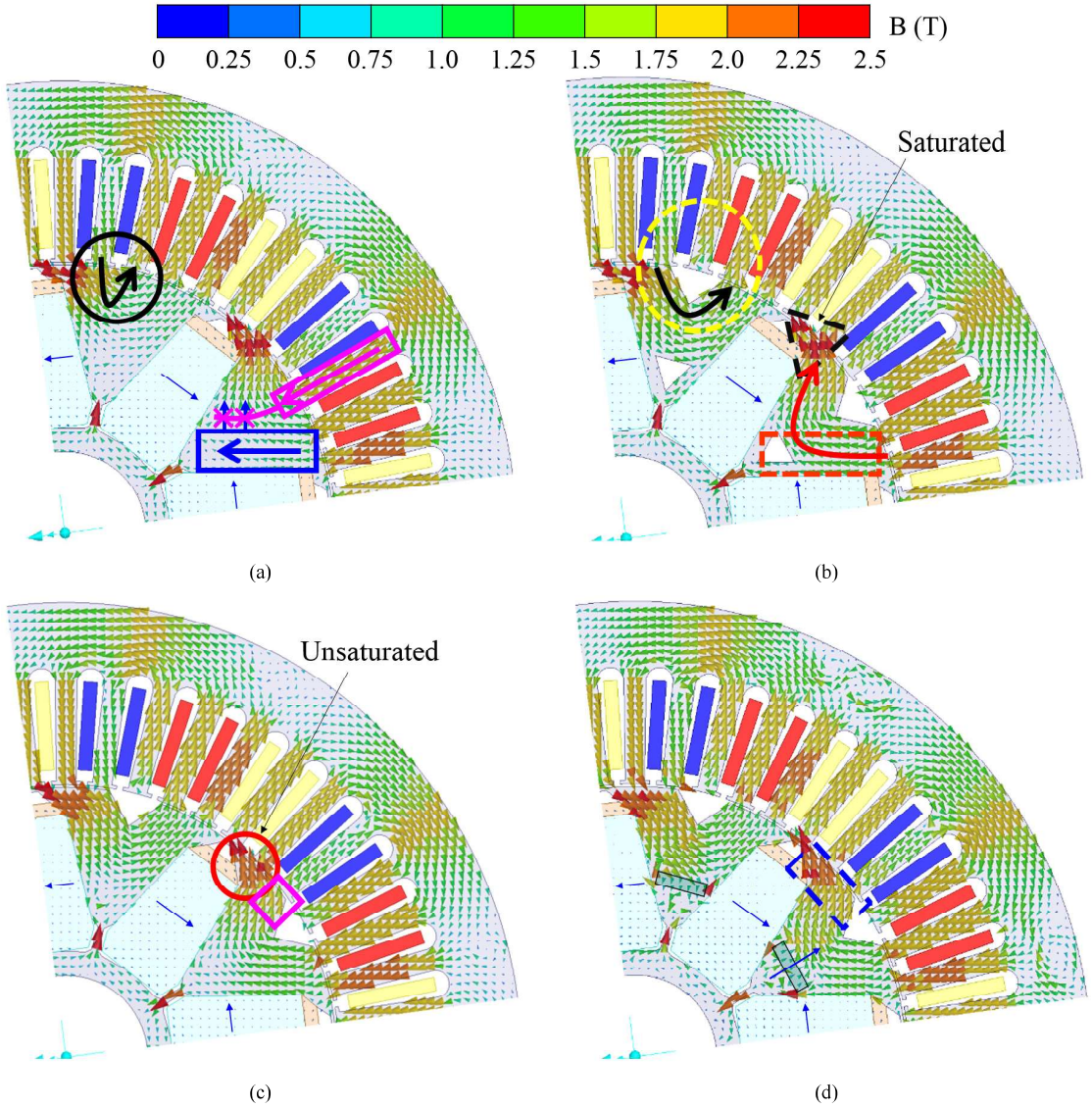

Fig. 3. Magnetic flux density (B-field) distribution of (a) without triangular void, (b) with triangular void, (c) with nonmagnetic cut, and (d) with nonmagnetic cut and supplementary magnet

producing a magnetic barrier. Furthermore, it is noted that the flux lines in a blue rectangular area in Fig. 3 (a) flow straight through the center of the rotor and not flow near to the air gap, wasting part of the flux. This is attributed to the winding flux from the middle slot, as shown in the pink rectangular area. The winding flux prevents the flux, that is generated by the coils (phase C) in red, from being used.

Thus, to mitigate these issues, the triangular cut was introduced between two RC magnets. As the yellow dotted circular area in Fig. 3 (b) displays, the flux that flown to the nearest neighboring slot in Fig. 3 (a) is blocked and redirected to the adjacent slots with much weaker density, reducing the effects of the magnetic barrier. Not only that, the triangular cut blocks the winding flux produced from the middle slot as shown in the pink rectangular area in Fig. 3 (a), therefore, allowing more flux lines, as shown in the orange dotted rectangular area, to be pulled from the stator winding flux, increasing the reluctance torque, as shown in Fig. 2. In addition to increased reluctance torque, the cogging torque, which arises from the interaction between the slot opening and PM flux, is halved by introducing the triangular cut.

Although the triangular cut and void enhance both the torque and torque ripple performance, the torque ripple of S-IPMSM-TCV is still too high (9.4 %) for the EV. The results show that this high torque ripple is caused by highly saturated areas, as shown in the black dotted triangular area in Fig. 3 (b). Generally, if the region is highly saturated, although high potential flux is achievable, severe distortions on air-gap flux and aggravation of torque pulsations occur [7]. Thus, to lessen the flux concentration in the region, the nonmagnetic materials were cut, as illustrated in the red circular area in Fig. 3 (c). As it shows, the flux in the red circular area is less concentrated,

TABLE III. TORQUE PERFORMANCE OF THE PROPOSED SPOKE-TYPE MOTOR WITH VARIOUS MAGNETS AT 20 °C

RC magnet \ FD magnet	LTP-MnBi	SrM	NdFeB
LTP-MnBi	188.2 Nm (6.9 %)	187.5 Nm (6.7 %)	191.9 Nm (9.0 %)
SrM	176.6 Nm (8.1 %)	175.6 Nm (9.5 %)	179.1 Nm (6.5 %)
NdFeB	238.7 Nm (11.3 %)	237.1 Nm (12.0 %)	240.3 Nm (10.2 %)

TABLE IV. TORQUE PERFORMANCE OF THE PROPOSED SPOKE-TYPE MOTOR WITH VARIOUS MAGNETS AT 125 °C

RC magnet \ FD magnet	LTP-MnBi	SrM	NdFeB
LTP-MnBi	181.1 Nm (6.9 %)	180.0 Nm (7.3 %)	185.3 Nm (6.2 %)
SrM	162.7 Nm (13.6 %)	161.2 Nm (15.1 %)	168.9 Nm (12.1 %)
NdFeB	224.9 Nm (15.4 %)	224.0 Nm (15.6 %)	225.6 Nm (15.3 %)

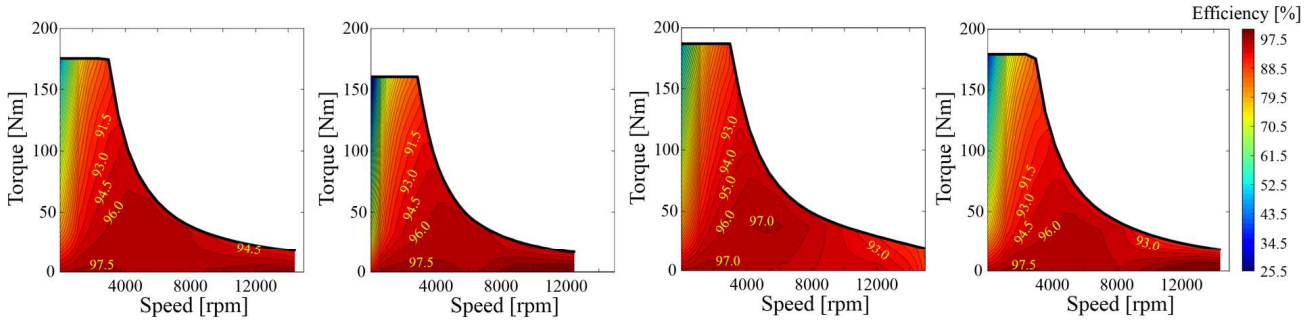

Fig. 4. Torque/speed characteristics and efficiency map of the conventional spoke-type motor at (a) 25 and (b) 125 °C and the proposed spoke-type motor with the MnBi/SrM combination at (c) 25 and (d) 125 °C.

resulting in a 9.7 % decrease in the reluctance torque ripple. However, the total torque also decreased.

To compensate for this loss in torque, an FD magnet was inserted between two RC magnets, allowing the more flux in the middle and upper part of the rotor, as shown in the blue dotted rectangular region in Fig. 3 (d), in the rotating direction. As a result, the total torque increased from 171.5 to 179.1 Nm. Also, the more concentrated flux in the blue dotted region results in torque ripple reduction. This is attributed to the uniform flux distribution on the edge of the rotor, resulting in more sinusoidal flux distribution on the air gap.

B. Effects of Different PMs Configuration on Torque Characteristics

Table III and IV summarize the torque performance of the proposed rotor with the three different PMs for FD and RC magnets at 20 °C and 125 °C, respectively. The torque and torque ripple of the conventional rotor are 175 Nm and 13.4 % at 20 °C, respectively, and 160 Nm and 19.7 % at 125 °C, respectively. The average torque of the proposed rotor is higher than the conventional rotor at 20 °C and 125 °C and shows linear proportionality with remanent flux density, B_r, of the RC and FD magnet. As for the torque ripple performance, the proposed rotor design for all PMs show less ripple than that of the conventional rotor for all PMs and exhibits a positive quadratic trend between the torque ripple and the B_r of the magnet at 20 and 125 °C.

Among the combinations of the PMs, MnBi (RC magnet) /MnBi (FD magnet) and MnBi/SrM show the most promising torque and torque ripple performance. It is noted that the proposed rotor with NdFeB for RC magnet showed highest torque ripple compared to three PMs. At 20 °C, the proposed rotor with MnBi/MnBi and MnBi/SrM combinations has not only increased the average torque by 7.5 and 7.1 %, respectively but also decreased the torque ripple by 48.5 and 50.0 %, compared to the conventional rotor. At 125 °C, the proposed rotor with MnBi/MnBi and MnBi/SrM combinations enhanced the average torque by 13.2 and 12.5 %, respectively, and reduced the torque ripple by 65.0 and 62.9 %, respectively. When the temperature increased to 125 °C from 20 °C, the torque of the proposed motor with MnBi/MnBi and MnBi/SrM was degraded by 3.8 and 4 %, respectively, while the torque ripple is increased by 0 and 9.0 %, respectively. Lastly, among the two combinations of the proposed rotor, MnBi/SrM was selected for further analysis, due to lower material cost with good motor performance.

C. Traction Motor Performance

Electric Machine Design Toolkits – R16, which is offered by Ansys Maxwell, is employed to evaluate the motor performance, such as torque characteristics, efficiency, and maximum speed, at 20 °C and 125 °C for the conventional and proposed spoke-type motor with the MnBi/SrM combination. Maximum torque per ampere (MTPA) control is applied until the motor reaches the base speed, while above the base speed, flux weakening control is utilized with consideration of the DC voltage and applied current constraints, which are 500 V and 177 A_{rms}, respectively. As for the voltage control type, space vector-pulse width modulation (SVPWM) is used. This control sets the maximum controllable voltage to 389 V.

Fig. 4 shows the torque and speed characteristics with an efficiency map at 20 and 125 °C of the conventional and proposed spoke-type motor with the MnBi/SrM combination.

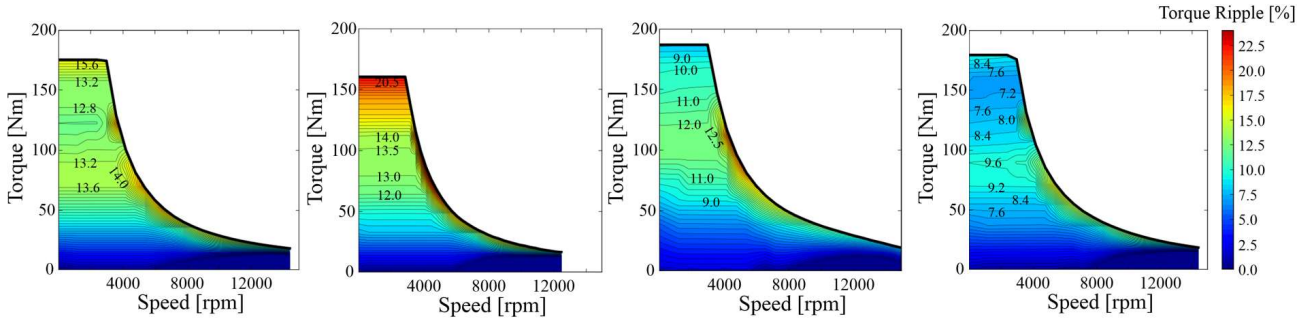

Fig. 5. Torque ripple performance for the conventional spoke-type motor at (a) 25 and (b) 125 °C and the proposed spoke-type motor with the MnBi/SrM combination at (c) 25 and (d) 125 °C.

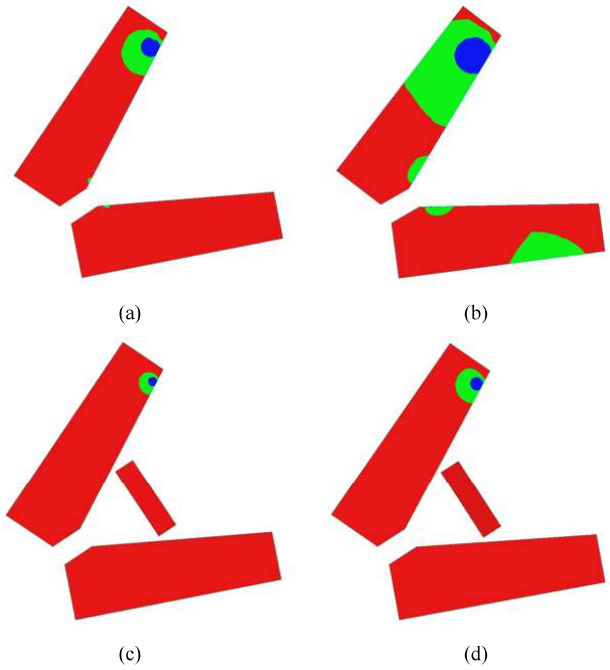

Fig. 6. Permanent magnet flux density of the conventional design (SrM) at (a) 20 °C and (b) 125 °C and proposed design (MnBi/SrM) at (c) 20 °C and 125 °C,

We realized that the conventional and proposed design could produce the maximum torque of 175 and 186.7 Nm until 3000 rpm at 20 °C, respectively, and 160.2 and 179.1 Nm until 2400 rpm at 125 °C, respectively, and sustain its operation up to 14,400 and 15,000 rpm at 20 °C, respectively, and 12,480 and 14,400 rpm at 125 °C, respectively. Compared to the conventional spoke-type motor with SrM magnet, the proposed spoke-type motor with the MnBi/SrM combination performs not only 11.7 and 19.1 Nm higher maximum torque but also 600 and 1,920 rpm higher maximum speed.

Fig. 5 shows the torque ripple performance of the conventional and proposed spoke-type motor with the MnBi/SrM combination at 20 °C and 125 °C. It clearly shows that the torque ripple of the proposed spoke-type motor is far less than that of the conventional motor in all torque and speed region.

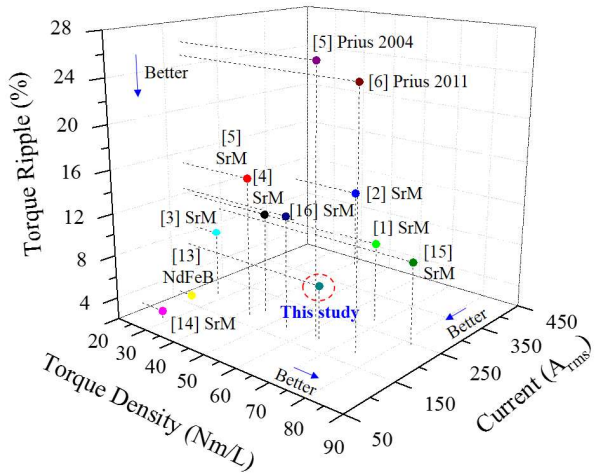

Fig. 7. Performance comparison based on torque ripple, torque density, and applied current at maximum torque and rated speed.

D. Demagnetization Analysis

A PM flux density above 0.1 T is highly suggested to prevent the irreversible demagnetization of the PMs. Thus, to assess the irreversible demagnetization, the areas where the PM flux density is below 0.1 T are investigated. Fig. 6 illustrates the distribution of flux density for the conventional (SrM) and proposed design (MnBi/SrM) at 20 and 125 °C. The areas where the PM flux density is below 0.1 T for the conventional and proposed rotor are 4.2 and 1.2 % at 20 °C, respectively, and 29.1 and 2.8 % at 125 °C, respectively. This suggests that the proposed motor is far better in preventing demagnetization than the conventional motor.

E. Performance Comparison with Prior Arts

The simulated torque characteristics of the proposed motor with applied current are compared with those of the reported motors, including the V-shaped IPMSM used in Toyota Prius, PM-assisted synchronous reluctance motor (PMASynRM), and S-IPMSM, with either Nd-Fe-B and SrM PM employed as shown in Fig. 7. The results show that although the V-shaped IPMSM used in Toyota Prius showed the highest torque density in range of 74-84 Nm/L with low applied current of 177 A_{rms}, it suffers from high torque ripple of 25-26.2 % and also requires

REPM. Although the PMASynRMs with RE-free PM showed moderate torque ripple of 11% and high torque density of 65 Nm/L in average, high applied current of 220 A_{rms} was required. Similarly, the S-IPMSM showed the reasonable torque density of 60 Nm/L and moderate torque ripple of 10 %, but demands high applied current of 275 A_{rms}. Compared to these motors, the proposed motor with MnBi for RC magnet and SrM for FD magnet showed not only high torque density of 65 Nm/L, but also lowest torque ripple of 7 % with low applied current of 177 A_{rms}, according to the simulation results.

IV. Conclusion

We have designed a rotor for spoke-type IPMSMs to minimize the torque ripple with enhanced average torque for EV applications. The designed motor with LTP-MnBi for the RC magnet and SrM for the FD magnet shows the increased torque by 7.1 % and 12.5 % at 20 °C and 125 °C, respectively, and decreased torque ripple by 50 % and 62.9 % at 20 °C and 125 °C, respectively. According to the demagnetization analysis, the proposed motor is far less vulnerable to irreversible demagnetization than the conventional motor. Therefore, this work opens a new avenue in the design of rare-earth free IPMSM for EV applications.

References

[1] W. Kakihara, M. Takemoto, and S. Ogasawara, "Rotor Structure in 50 kW Spoke-Type Interior Permanent Magnet Synchronous Motor with Ferrite Permanent Magnets for Automotive Applications," *2013 IEEE ECCE*, pp. 606-613, Sept. 2013.

[2] M. Kimiabeigi et al., "High-Performance Low-Cost Electric Motor for Electric Vehicles Using Ferrite Magnets," *IEEE Trans. Ind. Electron.*, vol. 63, pp. 113-122, Jan. 2016.

[3] S. J. Galioto, P. B. Reddy, A. M. El-Refaie, and J. P. Alexander, "Effects of Magnet Types on Performance of High-Speed Spoke Interior-Permanent-Magnet Machines Designed for Traction Applications," *IEEE Trans. On Ind. Appl.,* vol. 51, pp. 2148-2160, May/Jun. 2015.

[4] M. Obata, S. Morimoto, M. Sanada, and Y. Inoue, "Performance of PMASynRM with Ferrite Magnets for EV/HEV Applications Considering Productivity," *IEEE Trans. Ind. Appl.,* vol. 50, pp. 2427-2435, July/Aug. 2014.

[5] H. Cai, B. Guan, and L. Xu, "Low-Cost Ferrite PM-Assisted Synchronous Reluctance Machine for Electric Vehicles," *IEEE Trans. Ind. Electron.,* vol. 61, no. 10, pp. 5741-5748, Oct. 2014.

[6] Y. Guan, Z. Q. Zhu, I. A. A. Afinowi, J. C. Mipo, and P. Farah, "Comparison between induction machine and IPM for electric vehicle application," *COMPEL*, vol. 35, no. 2, pp. 572-585, Feb. 2016.

[7] W. Zhao, T. A. Lipo, and B. Kwon, "Torque Pulsation Minimization in Spoke-type IPM Motors with Skewing and Sinusoidal PM Configurations," *IEEE Trans. Magn,*. vol. 51, no. 11, pp. 8110804, Nov. 2015.

[8] C. Ruoff, "A closer look at torque ripple – minimizing its effects on electric machines," *Chargedvehicles*, Sept. 2011.

[9] N. Bianchi and S. Bolognani, "Design techniques for reducing the cogging torque in surface-mounted PM motors," *IEEE Trans. Ind. Appl.,* vol. 38, no. 5, pp. 1259-1265, Sep./Oct. 2002.

[10] N. Poudyal et al., "Processing of MnBi bulk magnets with enhanced energy product," *AIP Advances*, vol. 6, pp.056004, Feb. 2016.

[11] Hitachimetals, "NMF series" [Online]. Available: http://www.hitachimetals.com.

[12] Vacuum Schmelze, "Vacodym 890 TP datasheet," available at www.vacuumschmelze.com.

[13] E. Carraro and N. Bianchi, "Design and Comparison of IPMSM with non-uniform airgap and conventional rotor for EV applications," *IET Elec. Power Appl.* vol. 8, iss. 6, pp. 240-249, Jan. 2014.

[14] E. Carraro, N. Bianchi, S. Zhang, and M. Koch, "Performance Comparison of Fractional Slot Concentrated Winding Spoke Type Synchronous Motors with Different Slot-Pole Combinations," *Energy Conversion Congress and Exposition (ECCE)*, *2015 IEEE*, 6067-6074, 2015.

[15] Y. Li, D. Bobba, and B. Sarlioglu, "Design and Optimization of a Novel Dual-Rotor Hybrid Machine for Traction Application," *IEEE Trans. Ind. Electron.,* vol. 65, no. 2, pp. 1762, Feb. 2018.

[16] Y. Hwang, and J. Lee, "HEV Comparison of IPMSM With Nd Sintered Magnet and Heavy Rare-Earth Free Injection Magnet in the Same Size," *IEEE Trans. Appl. Supercond.* vol. 28, no. 3, pp. 5206405, Apr. 2018.